PERFORMANCE OF THE SYNCHROTRON RADIATION COLLIMATION SYSTEM IN THE FCC-ee INTERACTION REGION

G. Nigrelli*[1,2,3], K. André[4], M. Boscolo[3], G. Broggi[2], R. Bruce[2], S. Redaelli[2]
[1]Sapienza Università di Roma, Rome, Italy
[2]CERN, Geneva, Switzerland
[3]Istituto Nazionale di Fisica Nucleare, Rome, Italy
[4]ESRF, Grenoble, France

Abstract

The electron-positron Future Circular Collider (FCC-ee) is a proposed high-luminosity lepton collider which will operate at energies ranging from 45.6 to 182.5 GeV. Each beam will radiate up to 50 MW of synchrotron radiation power, whose disposal poses obvious challenges for the machine and for the experiments. The lattice design upstream of the interaction point employs weak dipoles and strong quadrupoles, within which the beam generates synchrotron radiation that could reach the detector and cause experimental background if not properly collimated. To mitigate this, a dedicated system of collimators and masks has been developed. This paper presents the performance of the FCC-ee synchrotron radiation collimation system in the interaction region in nominal conditions, in the presence of errors, and during top-up injection.

INTRODUCTION

The FCC-ee design study proposes a 90.7 km circumference electron–positron collider operating at beam energies between 45.6 and 182.5 GeV [1]. The high beam energy and current required to achieve the target luminosities cause significant synchrotron radiation (SR) emission, with each beam radiating up to 50 MW. While most radiation is generated in the arcs and absorbed by dedicated photon stoppers, SR control remains a challenge in the interaction region (IR). In the IR, SR is produced mainly by weak dipole magnets, by beam tails at the final quadrupoles and by the solenoid fringing field. The optics under study do not include solenoid fields, therefore this component is neglected in the following. Most photons are collinear with the beam trajectory and are absorbed in the photon dump [2, 3] downstream of the interaction point (IP), but a fraction of them can interact with the beam pipe or IR components and generate background in the detector. A dedicated SR collimation system has therefore been designed to intercept the SR and mitigate detector background [4].

This paper evaluates the performance of the SR collimation system for Z-mode operation at 45.6 GeV under nominal beam conditions, considering SR from both the beam core and halo and evaluating also the effect of orbit errors. The background from SR during top-up injection is also studied.

* giulia.nigrelli@cern.ch

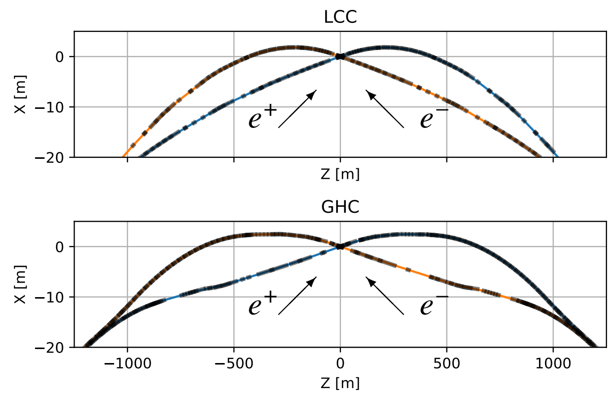

Figure 1: Interaction region layout for the LCC (top) and GHC (bottom) lattices.

INTERACTION REGION LAYOUT

Two lattice configurations, Global Hybrid Correction (GHC) V25.4 [5] and Local Chromaticity Correction (LCC) V106.1 [6], are considered. The IR lattice is common to all FCC-ee operating modes [7] but the IR layouts differ between GHC and LCC, as shown in the layouts of Fig. 1.

In both configurations, weak dipole magnets upstream of the interaction point and strong final focus quadrupoles steer and focus the beam in the IR. The two optics options have different layouts for dipoles and quadrupoles that cause different SR production. The GHC lattice also features reverse bends, which modify the SR direction. In the LCC lattice, the main SR sources are the dipoles B0AL and B0BL located about 26 m and 120 m upstream of the IP, while in the GHC lattice the dominant source is the dipole BWL located about 120 m from the IP.

SR COLLIMATION SYSTEM

A dedicated SR collimation system has been implemented in the IR to mitigate radiation reaching the detector. The system for LCC consists of five movable tungsten collimators (six for the GHC lattice) and two static tungsten masks, and is shown in shown in Fig. 2. The SR collimators are placed between the last dipoles (BWL for GHC and B0BL, B0AL for LCC) and the final focus quadrupoles. Two additional tungsten masks are added downstream of the magnets to provide additional shielding near the IP.

The SR collimator apertures respect the beam pipe aperture and betatron collimation hierarchy [8]. The beam pipe

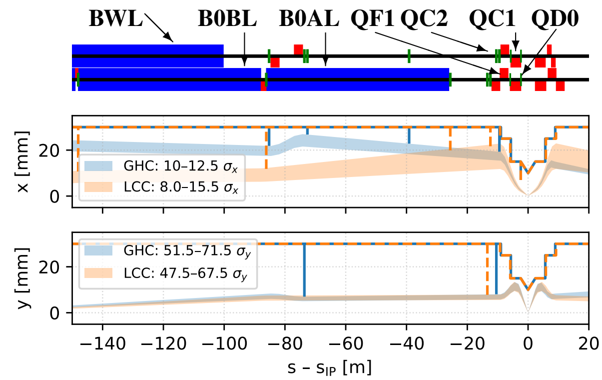

Figure 2: SR collimation system and aperture profile for the LCC and GHC lattice. The IP is located at $s = 0$ m.

radius decreases from 30 mm upstream of the final doublet (QC2 and QC1 for GHC, and QF1 and QD0 for LCC) to 25 mm at QC2/QF1, to 15 mm at QC1/QD0, and to 10 mm at the IP. The machine aperture bottlenecks are $15.5\sigma_x/67.5\sigma_y$ for LCC and $12.5\sigma_x/71.5\sigma_y$ for GHC. The primary betatron collimator apertures are set to $8\sigma_x/47.5\sigma_y$ for LCC and $10\sigma_x/51.5\sigma_y$ for GHC to protect these aperture bottlenecks [9]. Therefore, the SR collimator aperture is set to the same normalized opening in σ as the aperture bottleneck in order to maintain the collimation hierarchy while protecting the final quadrupoles from direct SR hits. The masks are arranged as follows: a circular one between the final focus quadrupoles, where the aperture reduces from 25 to 15 mm, and a second mask composed of two horizontal jaws with a 7 mm gap, positioned 2.3 m upstream of the IP. The upstream collimators intercept the SR from the dipoles, while the masks protect against photons produced in the dipoles and final focus region.

SIMULATION SETUP

The IR geometry for both lattice configurations was implemented in BDSIM [10], based on the GEANT4 toolkit, as in [4]. The lattice and optics were imported from MAD-X, allowing flexibility in the number of elements included in the model. The model includes the SR collimation system described above and a realistic vacuum chamber with winglets [11]. However, the model lacks a realistic description of the magnet geometry, tunnel, detector cavern, and the central chamber where the separate beam pipes merge into a single elliptoconical chamber. This may affect the particle distribution at the detector outside of the beam pipe, however, this study focuses only on photons propagating within the beam pipe, believed to be the most important contribution. The background caused by particles outside of the beam pipe will be studied in future work.

The simulation is performed by initializing a positron beam distribution at the model entrance and tracking it through the geometry and magnetic fields, while generating and tracking photons. The output is the distribution of photons impinging on the beam pipe. X-ray reflection on the beam pipe surface was included [12], assuming a surface roughness of 100 nm.

Table 1: Parameters for GHC and LCC Lattice Configurations at Z-mode Operation

Parameter	GHC V25.4	LCC V106
Beam energy [GeV]	45.6	45.6
Beam current [mA]	1281	1281
Horizontal emittance ε_x [nm rad]	0.74	0.70
Vertical emittance ε_y [pm rad]	2.5	2.6
Energy spread σ_E/E [%]	0.129	0.134
Bunch length σ_z [mm]	16.3	16.7
β_x^* [mm]	90	90
β_y^* [mm]	0.7	0.7
l^* [m]	2.4	2.4

The SR photon distribution was evaluated for several beams, including the core and halo of the nominal, beam distributions resulting from orbit errors, as well as the injected beam during top-up injection. The beam core was modeled as a six-dimensional Gaussian distribution matched to the optics at the IR entrance using Table 1 parameters, assuming 99% of the beam intensity in the core. The halo distribution was generated with the Sands quantum lifetime model [13]. A beam lifetime of 5 minutes was assumed to represent a conservative scenario, with the halo population normalized to 1% of the nominal beam intensity. Orbit error scenarios were generated using transverse offsets (x, p_x, y, p_y) extracted from lattice simulations including random errors and the subsequent orbit corrections [14], which were applied to the nominal beam distribution using 20 random seeds. As simulated orbit corrections were only available for the GHC lattice, only this case has been considered so far. Injected beam conditions were simulated using dedicated tracking simulations [15]. The particle distribution was recorded at the last upstream dipole and summed over 100 machine turns after injection, and then used as input for the BDSIM simulations.

RESULTS

The performance of the SR collimation system was evaluated by analyzing the incident power on the aperture along the interaction region components. Results are presented for the two lattices and for the different beam scenarios.

Figure 3 shows the incident SR power along the IR for a beam composed of both core and halo particles. The SR collimation system effectively protects the detector in both lattice configurations by concentrating losses on the collimators and masks. The total SR incident power is $\sim$ 20 kW, integrated over $s \in [-125, 75]$ m. The halo contributes $\sim$ 2 kW. The incident SR power in the central chamber ($\pm$10 cm around the IP) remains below 1 W/m. However, this is the main source of detector background, primarily due to the halo contribution, which increases the incident power by a factor of 3 (1.3) for LCC (GHC). Overall, the LCC lattice produces about 10% more synchrotron radiation than GHC. In addition, the radiation is more concentrated within the detector cavern region ($\pm$30 m), about 40% more than GHC. In both lattices, the masks intercept approximately 100 W of SR power. Most of this power originates from the core beam (94% for LCC and 76% for GHC), as most of the halo-induced SR is absorbed downstream of the IP. The im-

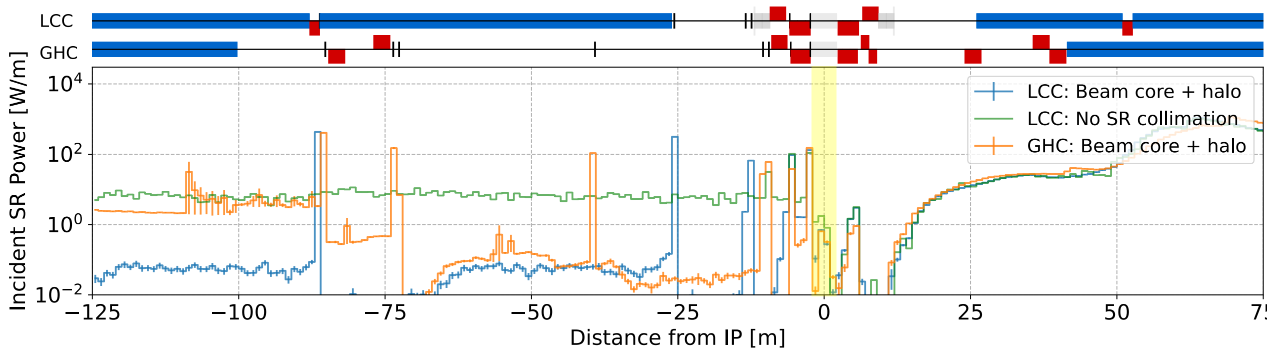

Figure 3: Simulated SR power incident in the IR for beam core and halo (5 min lifetime) in the GHC and LCC lattices. The green line shows the LCC case without collimators; the yellow band marks the region of interest for background.

pact distributions differ: in GHC photons impact both mask jaws due to the reverse bends, while in LCC the radiation is mainly focused on a single jaw. Halo particles emit most of their SR in the final focus quadrupoles, leading to a more symmetric photon distribution between the mask jaws.

The performance of the SR collimation system was also evaluated in the presence of orbit errors. Orbit distortions could increase the amount of SR produced, particularly in the final focus quadrupoles. Simulation shows that the considered orbit errors neither significantly alter the SR distribution along the IR nor increase the total SR emission by more than 0.2% on average.

The performance of the SR collimation system was also evaluated for photons produced by the injected beam during top-up injection. Since the injection is performed off-momentum, large transverse oscillations are not expected in the IR. However, the simulated distribution exhibits heavy transverse tails that can generate additional SR.

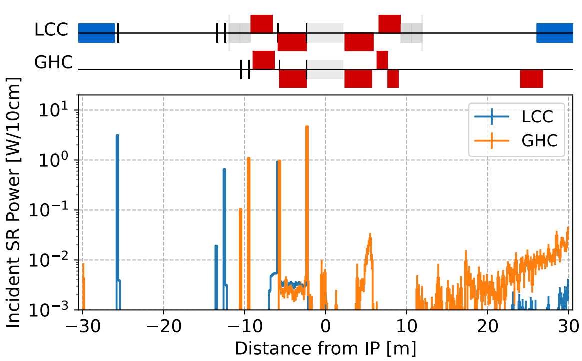

Figure 4: Incident SR power along the IR for the injected beam distribution.

Figure 4 shows the incident SR power along the IR, with the total remaining below 4 kW. Photons within the detector region could still contribute to background. Nevertheless, the incident power from the injection process remains well in the shadow of the one from the circulating beam.

Table 2 summarizes the total incident SR power in different regions of the IR for the considered scenarios. The ranges are defined as follows: IR $[-125, 85]$ m, cavern $[-30, 30]$ m, detector $[-10, 10]$ m, and central chamber (CC) $[-0.09, 0.09]$ m with respect to the IP. Only a small

Table 2: Incident SR Power (in W) in Several Regions of the IR for the Two Lattices

	Core		Core+Halo		Injection	
Region	**LCC**	**GHC**	**LCC**	**GHC**	**LCC**	**GHC**
IR $[10^4]$	2.1	1.8	2.2	2.0	0.0012	0.36
Cavern $[10^2]$	6.0	2.4	7.7	4.6	0.061	0.076
Detector $[10^2]$	2.2	1.5	2.4	1.9	0.023	0.058
CC $[10^{-1}]$	1.68	3.45	5.25	4.55	0.0225	0.0286
Mask QC1 $[10^2]$	1.24	1.22	1.32	1.61	$< 10^{-4}$	$< 10^{-4}$

fraction reaches the central chamber (±0.09 m), where the incident power remains below the W level for all scenarios. Despite this, such levels remain challenging for the tracker detector located just above the central beam pipe. Preliminary occupancy studies indicate levels exceeding the dominant luminosity background [16]. Further simulations will be performed to develop mitigation strategies.

The results also highlight differences between the two lattice configurations: LCC produces higher SR power under nominal conditions, whereas GHC exhibits a larger contribution during injection. These evaluations will support the SR mask design, which, being located inside the cryostat, requires careful study.

CONCLUSION

The performance of the SR collimation system in the FCC-ee IR was evaluated for two lattice configurations, GHC V25.4 and LCC V106. The total SR power produced in the IR is approximately ~ 20 kW. The system effectively protects the detector region from SR generated in the upstream dipoles and final focus magnets. The LCC lattice produces 10% more SR, which is more concentrated in the detector cavern region. The SR power in the central chamber remains below O(W/m) in all cases. The dominant source of SR background is radiation emitted by the beam halo at the final focus quadrupoles and deposited in the central chamber, which alone accounts for up to 70% of the incident power. Realistic orbit errors do not significantly alter these results, and the SR power from the injected beam is much smaller than from the the circulating one. Further studies will focus on detector simulations to estimate the synchrotron radiation background.

REFERENCES

[1] A. Abada *et al.*, "FCC-ee: The Lepton Collider, Future Circular Collider Conceptual Design Report Vol. 2", *Eur. Phys. J. ST*, vol. 228, pp. 261–623, 2019. doi:10.1140/epjst/e2019-900045-4

[2] M. Boscolo and A. Ciarma, "Characterization of Beamstrahlung Radiation at FCC-ee", *Phys. Rev. Accel. Beams*, vol. 26, p. 111002, 2023. doi:10.1103/PhysRevAccelBeams.26.111002

[3] A. Frasca *et al.*, "Radiation environment at FCC-ee experimental insertion regions", *Phys. Rev. Accel. Beams*, to be published. doi:10.1103/9j2q-zqxd

[4] K. D. J. André *et al.*, "Status of Synchrotron Radiation Studies in the FCC-ee Interaction Region", in *Proc. IPAC'24*, 2024. doi:10.18429/JACoW-IPAC2024-WEPR09

[5] K. Oide *et al.*, "Design of Beam Optics for FCC-ee Collider Rings", *Phys. Rev. Accel. Beams*, vol. 19, p. 111005, 2016. doi:10.1103/PhysRevAccelBeams.19.111005

[6] P. Raimondi *et al.*, "Local Chromatic Correction Optics for FCC-ee", *Phys. Rev. Accel. Beams*, vol. 28, p. 021002, 2025. doi:10.1103/PhysRevAccelBeams.28.021002

[7] M. Boscolo *et al.*, "Status of the FCC-ee Interaction Region Design", *EPJ Tech. Instrum.*, vol. 12, p. 4, 2025. doi:10.1140/epjti/s40485-025-00117-3

[8] G. Broggi, "FCC-ee Collimation System Design", Ph.D. thesis, Sapienza Università di Roma, 2026.

[9] F.F. Van der Veken *et al.*, "Proposed Collimation Layout for the FCC-ee with Local Chromaticity Correction Optics", presented at the *IPAC'26*, Deauville, France, 2026, paper MOP1052, this conference.

[10] L. J. Nevay *et al.*, "BDSIM: An Accelerator Tracking Code with Particle–Matter Interactions", *Comput. Phys. Commun.*, vol. 252, p. 107200, 2020. doi:10.1016/j.cpc.2020.107200

[11] R. Kersevan, "Vacuum system and photoelectron distributions in the collider", presented at *FCCIS'23 WP2 Workshop*, Rome, Italy, 2023,

[12] H. Burkhardt, "X-ray reflection process", presented at 28^{th} *Geant4 Collaboration Meeting*, Sapporo, Japan, 2023,

[13] M. Sands, "The Physics of Electron Storage Rings: An Introduction", in *Proc. Int. School of Physics "Enrico Fermi"*, pp. 257–411, 1969.

[14] S. S. Jagabathuni *et al.*, "FCC-ee Optics Tuning Studies with pyAT and Xsuite", in *Proc. IPAC'25*, 2025. doi:10.18429/JACoW-IPAC2025-MOPM037

[15] G. Nigrelli *et al.*, "Injection Background Studies at FCC-ee", presented at the *IPAC'26*, Deauville, France, 2026, paper MOP1050, this conference.

[16] A. Ilg, "Studies of backgrounds in vertex detectors", presented at 9^{th} *FCC Physics Workshop*, Munich, Germany, 2026,